Karman Vortex Shedding: Friend or Foe of the Structural Dynamicist?

L. E. Ericsson*
Lockheed Missiles & Space Company Inc., Sunnyvale, California

An analysis including the coupling between Karman vortex shedding and body motion has been performed for rectangular cross sections. The analysis shows how the Karman vortex shedding can eliminate the large-amplitude response caused by so-called galloping or stall flutter over significant portions of the reduced velocity region. However, in the absence of the galloping and stall flutter phenomenon, i.e., for conditions where the cross section has positive aerodynamic damping, the Karman vortex shedding will be the flow phenomenon causing divergent oscillations.

Nomenclature

c = two-dimensional chord length, $=D$ for a circular cylinder
D = cylinder diameter
f = frequency of oscillating body
f_v = frequency of Karman vortex shedding
f_{v0} = f_v for stationary flow conditions
h = cross-sectional height or thickness
S = Strouhal number, $=fh/U_\infty$ or fD/U_∞
t = time
Δt = time lag
$U, \bar{U}$ = horizontal and convection speeds, respectively
$\bar{V}$ = reduced velocity, $=S^{-1}$
x = chordwise distance from the leading edge
z = vertical displacement, positive downward
$\dot{z}$ = $\partial z/\partial t$
α = angle of attack
Δ = amplitude
ξ = dimensionless x coordinate, $=x/c$
ρ = air density
ϕ = phase angle, $=\omega\Delta t$
$\omega, \tilde{\omega}$ = oscillation frequency; $\omega=2\pi f$, $\tilde{\omega}=\omega c/U_\infty$

Subscripts

cr = critical, $f=f_{v0}$
sp = separation point
SB = stability boundary
v = vortex
w = wake
0 = stationary conditions
∞ = freestream conditions

Introduction

In the aeroelastic analysis of the Space Shuttle cable trays,[1,2] it was concluded that in some cases they would be subject to dynamic instability of the stall flutter type[3] and therefore had to be protected by flow ramps. Whereas the moderate ramp needed to protect the LO_2 cable tray never presented any difficulties in regard to launch vehicle handling, the bulkier solid-rocket booster (SRB) cable-tray fairings complicated the Shuttle stacking procedure and required very time-consuming manual work on the launch pad to complete the installment. Thus, the SRB trays were redesigned to eliminate this time delay of approximately two days.

The new design moved the rectangular ($c/h=1.96$) SRB cable tray closer to the surface of the external tank, resulting in a much stiffer support structure. The natural frequencies, both in bending and torsion, then fell in the Karman vortex shedding range and a new analysis had to be performed to determine how the aeroelastic stability of the new SRB cable tray was affected by Karman vortex shedding.[4] The results showed that, depending upon the natural frequency of the SRB cable tray, the Karman vortex shedding could eliminate or worsen the stall flutter problem. The present paper shows the fluid-mechanical reasons for this friend-foe behavior.

Karman Vortices

Judging by experimental results, obtained for circular cylinders in close proximity to a ground plane,[5] the rectangular cross section of the SRB cable tray, $c/h\approx 2$, can be expected to generate Karman vortices even in the presence of the external tank surface, and the Karman vortex shedding frequency should be close to that for a cross section free of ground plane interference. Furthermore, the Karman vortex shedding phenomenon remains essentially the same throughout the subsonic speed range.[6] Thus, incompressible flow results[7-9] for $c/h=2$ rectangular prisms apply to the SRB cable tray.

For cross sections with $c/h<2.5$, negative lift slopes have been measured,[11] resulting in an instability in bending or plunging oscillations, which often is called "galloping instability."[12] The maximum limit cycle amplitude of such oscillations can be predicted analytically.[12,13] The experimentally observed amplitude[14] falls, below this prediction, as expected (Fig. 1). However, the expected galloping behavior is realized for $\bar{V}\gg\bar{V}_{cr}\approx 11$ only.

It can be seen that for oscillation frequencies above the Strouhal frequency, i.e, for $\bar{V}<\bar{V}_{cr}$, where $\bar{V}_{cr}=S_{v0}^{-1}$, the response amplitude goes to zero. A similar behavior has been observed for a circular cylinder[15] (Fig. 2). Note that the Karman vortex shedding locks on to the cylinder oscillation over a large velocity range. It is shown in Refs. 16 and 17 that at $\bar{V}<\bar{V}_{cr}$ the Karman vortex shedding has a damping influence on the cylinder oscillation, whereas the influence is the opposite for $\bar{V}>\bar{V}_{cr}$.

The coupling between body motion and Karman vortex shedding responsible for the so-called lock-on phenomenon, with associated positive and negative damping effects, is a result of moving-wall effects on the boundary-layer development between the stagnation and separation points.[10,17] It is shown in Ref. 18 how similar moving-wall effects exist for the

Presented as Paper 85-0661 at the 26th AIAA/ASME/ASCE/AHS Structures, Structural Dynamics and Materials Conference, Orlando, FL, April 15-17, 1985; received May 3, 1985; revision received April 7, 1986.

*Senior Consulting Engineer. Fellow AIAA.

rectangular cross section. These effects should, of course, also be present in the galloping case when $\bar{V} \gg \bar{V}_{cr}$. The flow diagram in Fig. 3 illustrates how the moving-wall effect on the front face would amplify the separation asymmetry existing at a certain flow inclination $\dot{z}/U_\infty$ generated by the plunging motion.

Figure 3 suggests that near the critical body length for flow reattachment, $c/h \approx 2.5$, the moving-wall effect could cause flow separation on the top side even for $c/h > 2.5$. Parkinson's results for galloping rectangular cross sections[19] (Fig. 4) show such moving-wall effects. Static measurements indicate that the lift slope at $\alpha = 0$ is negative for $c/h < 2.5$,[11] whereas the galloping results in Fig. 4 show that complete flow separation was occurring on the top side, as sketched in Fig. 3, even for a rectangular cross section with $c/h = 3$. Likewise, the extension below $c/h = 1$ of the galloping region in Fig. 4 could, in part, be caused by flow reattachment on the bottom side due to moving-wall effects (see Fig. 3).

Thus, the coupling between body motion and flow separation and, hence, between body motion and Karman vortex shedding, is well documented. In addition, there is a coupling between the shed vortices and the body motion, which in the case of the circular cylinder may have been of less importance since there is not a suitable aft body on which to induce a lift force. For the rectangular cross section, however, the situation is very different (Fig. 5). The vortex is at the end of the shed "upstroke." This is consistent with the phase-lag characteristics for a rectangular cylinder, as will be demonstrated. Note that the circulation lift is developed on the plunging "downstroke."

The phase angle $\phi_v = \omega \Delta t_v$ shown in Fig. 5 determines how the vortex-induced suction force will affect the oscillating rectangular cross section. When the force (open vector in Fig. 5) is in the direction of the translatory velocity (solid vector in Fig. 5), it has an undamping effect, driving the translatory oscillation, adding to the moving-wall effects discussed previously.

When the chord length is increased, say, to $c/h = 4$, one would expect the response to change from the galloping type (Figs. 1 and 4) and become similar to the one experienced by the circular cylinder (Fig. 2), where the response occurs over a limited $\bar{V}$ range due to the negative aerodynamic damping generated by the Karman vortex shedding. Experimental results[20] for $c/h = 3$ and 4 are in agreement with such expectations (Fig. 6). [The fact that a $c/h = 3$ rectangular cross section exhibited the galloping behavior in one test[19] (Fig. 4) and not in another[20] (Fig. 6) illustrates how sensitive even these bluff-body flows are to Reynolds number and freestream turbulence. Differences in three-dimensional flow effects related to support design is another source of flow variations.] At $c/h = 2$ and 2.5 a similar type of response is obtained at supercritical frequencies, $\bar{V} \approx \bar{V}_{cr}/2$. See also the results in Fig. 1 for a $c/h = 2$ rectangle.

The experimental results in Ref. 11 showed that the pitching-moment slope for a midchord rotation point remained negative for all of the tested rectangular cross sections,

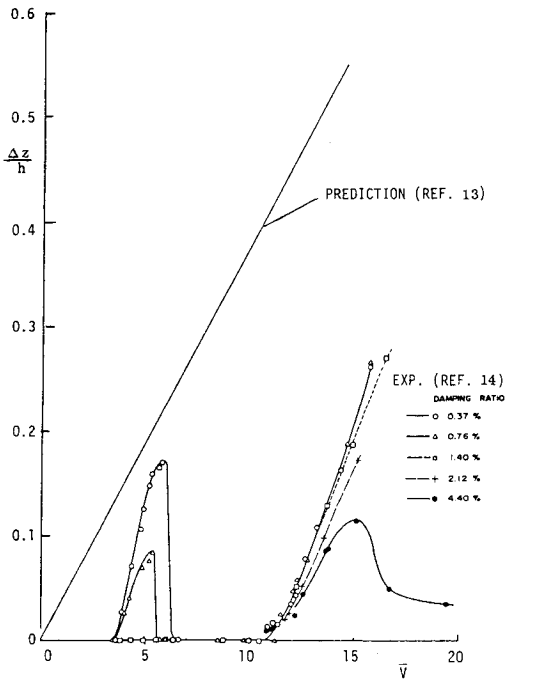

Fig. 1 Response characteristics of a $c/h = 2$ rectangular cylinder.

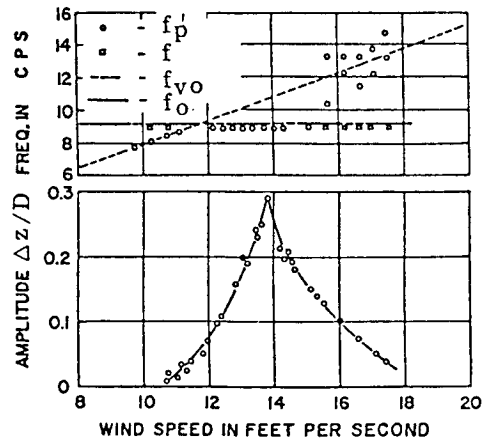

Fig. 2 Response of a circular cylinder at subcritical Reynolds number.[15]

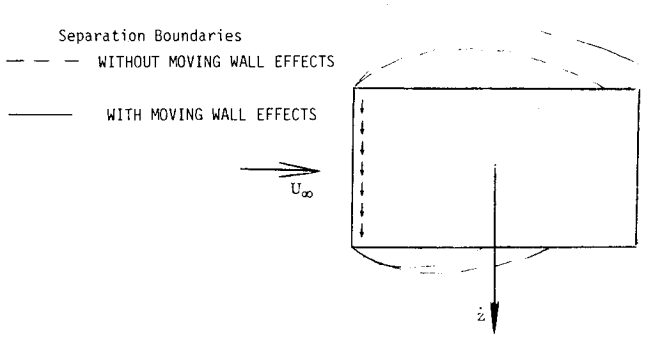

Fig. 3 Moving-wall effect on a plunging rectangular cross section.

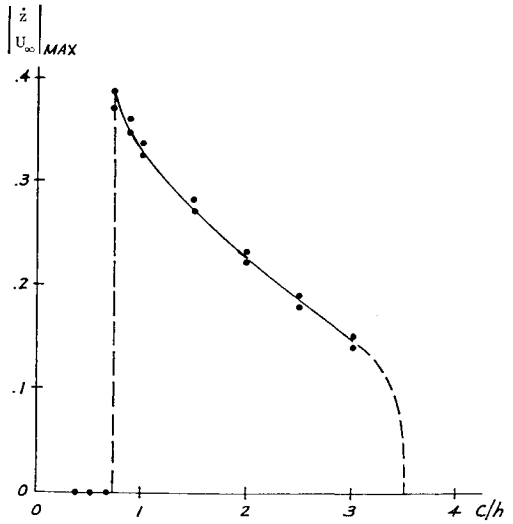

Fig. 4 Galloping cable data for rectangular cross sections.[19]

$1 \le c/h \le 4$. It is shown in Refs. 1 and 2 that due to the effect of flowfield time lag the separation-induced statically stabilizing effects are destabilizing dynamically. Consequently, it is no surprise that the torsional instability (stall flutter) characteristics for a $c/h = 3$ rectangle (Fig. 7b) are similar to the bending (galloping) ones for a square cross section[20] (Fig. 7a). Aside from this general similarity in the amplitude divergence characteristics, the details of the stability boundaries[20] are very different for torsional and bending oscillations (compare Figs. 8 and 6). A simple analysis applying dynamic stall concepts[21,22] will be performed to explain these differences.

Analysis

It is shown in Refs. 21 and 22 that for a stalling airfoil the lift is lagging the instantaneous angle of attack. For pitch oscillations at frequency ω, the corresponding phase lag is $\phi_w + \phi_{sp}$, where ϕ_w is the Karman-Sears wake lag ($\phi_w = 1.5\bar{\omega}$) and ϕ_{sp} is the lag due to the moving separation point effect. For the sharp-edged rectangular cross section discussed here, the separation point remains fixed and $\phi_{sp} = 0$. After this delay of flow separation the leading-edge vortex is "spilled," traveling downstream over the chord at a mean convection velocity $\bar{U}_v$ that is only a fraction of the freestream speed.[23,24] Thus, before the spilled vortex reaches the chordwise position $x_v = \xi_v c$, an additional phase lag $\phi_v = (U_\infty/\bar{U}_v)\xi_v\bar{\omega}$ takes place. It is shown in Ref. 18 that, for $c/h < 2.5$, the mean convection velocity of the spilled Karman vortex is $\bar{U}_v = 2U_\infty/7$. Thus, with $\bar{\omega} = 2\pi S$ and $c/h = 2\pi(c/h)/\bar{V}$, the total phase lag $\phi = \phi_w + \phi_v$ becomes

$$\phi = (3 + 7\xi_v)\pi(c/h)/\bar{V} \tag{1}$$

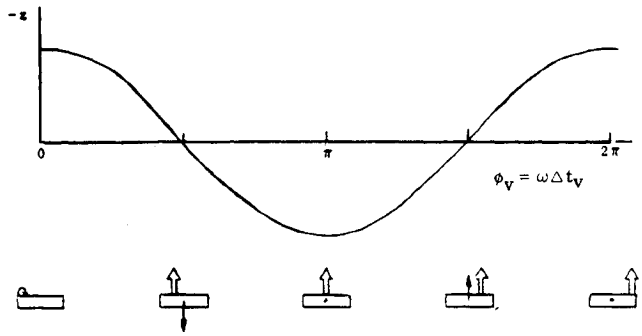

Fig. 5 Conceptual vortex-induced effect.

Plunging Oscillations

Figure 9 illustrates the variation of z and $\dot{z}$ with time. Also shown is the phase lag $\phi_w = \omega\Delta t_w$ occurring before the lift is realized, which was generated earlier at time $t - \Delta t_w$. As in Fig. 5, the open vector denotes the force vector (in this case for negative rather than positive lift slope, as in Fig. 5) and the solid vector denotes the translational velocity of the cross section. The figure shows that a damping interaction from the Karman vortex shedding is obtained when ϕ exceeds $\pi/2$. The earliest this can occur is when the vortex is still located at the leading edge, i.e., when $\phi = \phi_w$ and $\xi_v = 0$ in Eq. (1). Thus, the Karman vortex shedding has a damping effect when

$$\bar{V} < 6(c/h) \tag{2}$$

In Fig. 10 the stability boundary at $\alpha = 0$ for plunging rectangular cross sections is plotted in a somewhat different format than that in which the experimental results[9,20] were originally presented (Fig. 6). This is done to attain a more direct comparison with the galloping characteristics, as shown in Fig. 1. Also shown in Fig. 10 is the critical velocity $\bar{V}_{cr} = S_{v0}^{-1}$ for the Karman vortex shedding from a stationary cross section. It can be seen that the result is similar to that for a circular cross section (Fig. 2) in a damping influence from the Karman vortex shedding is obtained when the cross section oscillates at a higher frequency than that for Karman vortex shedding from a stationary section, i.e., when $\bar{V} < \bar{V}_{cr}$. As $\xi_v = 0$, the stability boundary $\bar{V}_{SB}$ is close to the critical value

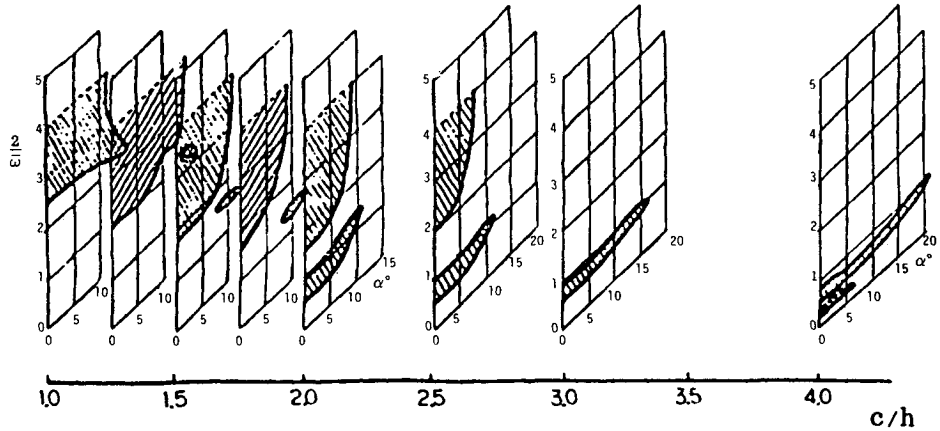

Fig. 6 Stability boundaries for bending oscillations of rectangular cylinders.[20]

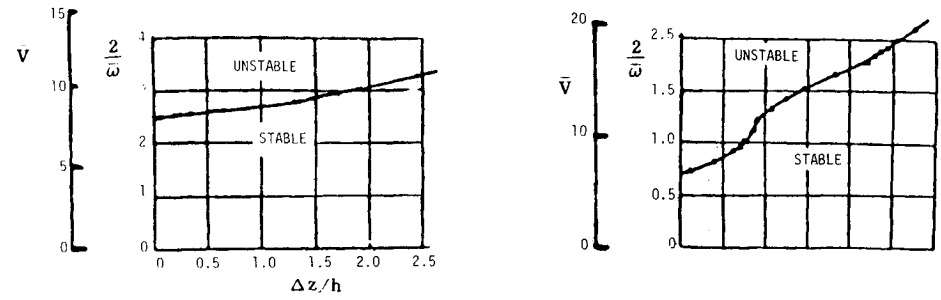

a. Bending Oscillations, c/h = 1 b. Torsional Oscillations, c/h = 3

Fig. 7 Amplitude divergence characteristics for rectangular cylinders.[20]

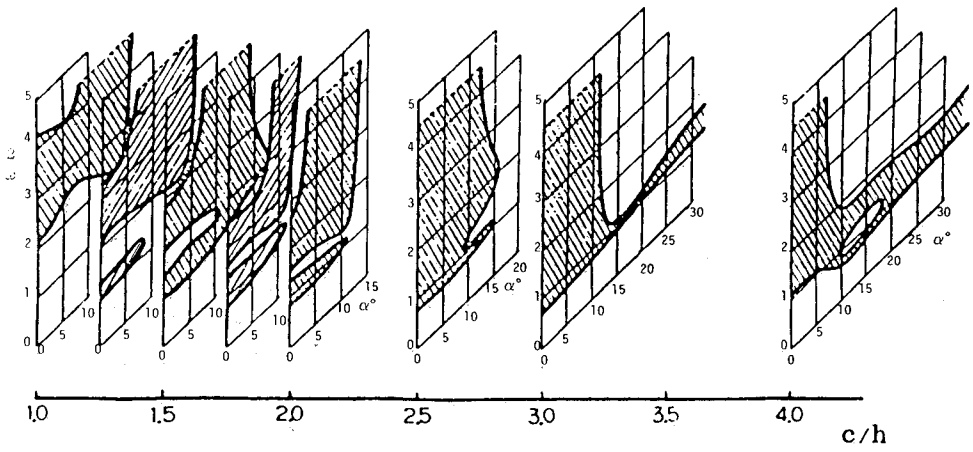

Fig. 8 Torsional stability boundaries for rectangular cylinders.[20]

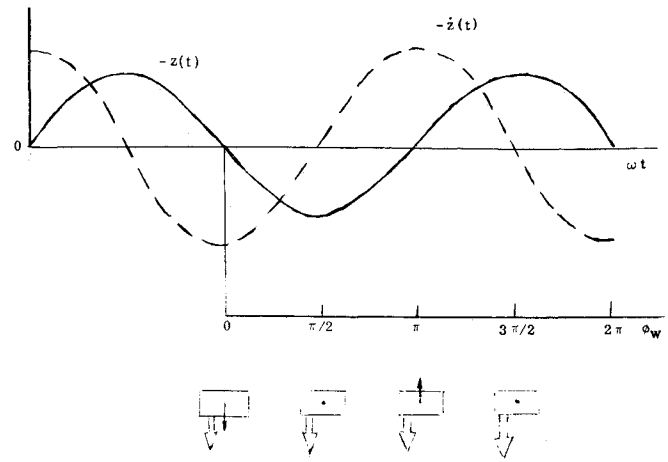

Fig. 9 Conceptual effect of vortex-induced force for bending oscillations.

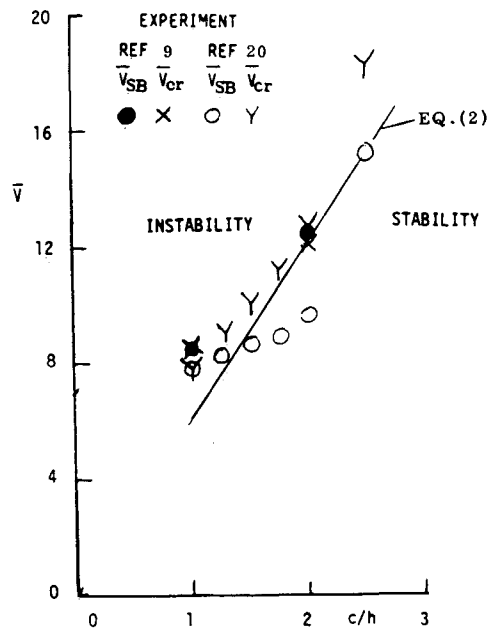

Fig. 10 Predicted and measured stability boundaries at $\alpha = 0$ for harmonic bending response of rectangular cross sections to Karman vortex shedding.

$\bar{V}_{cr} = S_{v0}^{-1}$. Figure 10 shows that Eq. (2) predicts the experimental stability boundary rather well.

Referring again to Fig. 1, one can get a certain appreciation for the magnitude of this damping effect. At $\bar{V} > 15$, where the coupling with the Karman vortex shedding has ceased, a mechanical damping as large as 4.4% of critical is needed to overcome the negative aerodynamic damping leading to the galloping instability. That must at least be the magnitude of the damping due to the Karman vortex shedding at $7 < \bar{V} < 11$, as the amplitude goes to zero there rather than remaining finite, as for $\bar{V} > 15$. When considering the fact that none of the Space Shuttle cable trays had structural damping exceeding 1% of critical,[1,2] one gets some appreciation of the importance of correctly accounting for the coupling between body motion and Karman vortex shedding.

Torsional Oscillations

As was observed earlier, the torsional stability boundary differs substantially from that for the plunging oscillations. The main effect of the Karman vortex shedding is to create a region of instability (Fig. 8). Experimental results[25] indicate that the aerodynamic damping in pitch around midchord is slightly positive for $c/h = 2$. Since there is always an appreciable amount of external (mechanical) damping present in dynamic tests, such as those giving the results shown in Fig. 8, one can understand one aspect of the results, i.e., the only measurable effect of the Karman vortex shedding is its dynamically destabilizing effect, as the oscillations are damped in the absence of any vortex shedding effects.

Figure 11 shows the variation of α and $\dot{\alpha}$ with time and the phase lag $\phi = \phi_w + \phi_v$. Two locations for the vortex-induced force are shown—one forward of the torsional axis and one aft. For the forward location, a dynamically destabilizing vortex-induced effect is obtained for $\phi < \pi$. With the lift concentrated at the quarter-chord location, $\xi_v = 0.25$ in Eq. (1), which would include the initial vortex growth period of the spilled vortex,[22] one should get the maximum torsional moment for the tortional axis located at midchord. Thus, Eq. (1) gives the following stability condition for $\phi < \pi$:

$$\bar{V} > 4.75(c/h) \tag{3}$$

For the aft force location, a dynamically destabilizing effect of the vortex-induced force is obtained for $\phi > \pi$. According to Ref. 22, the maximum magnitude of the vortex-induced torsional moment is obtained for $\xi_v = 1$. Thus, the following instability condition is obtained from Eq. (1) for the aft force location:

$$\bar{V} > 10(c/h) \tag{4}$$

Equations (3) and (4) give predictions that are in good agreement with the experimental results[9,20] (Fig. 12), especially when considering the data spread between Refs. 9 and 20, and the presence of mechanical damping in the test. Going

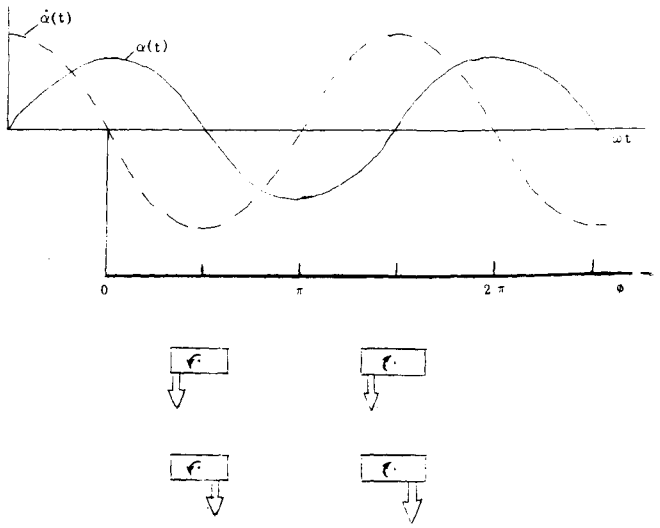

Fig. 11 Stability boundaries for harmonic torsional response at $\alpha = 0$ to Karman vortex shedding of rectangular cross sections.

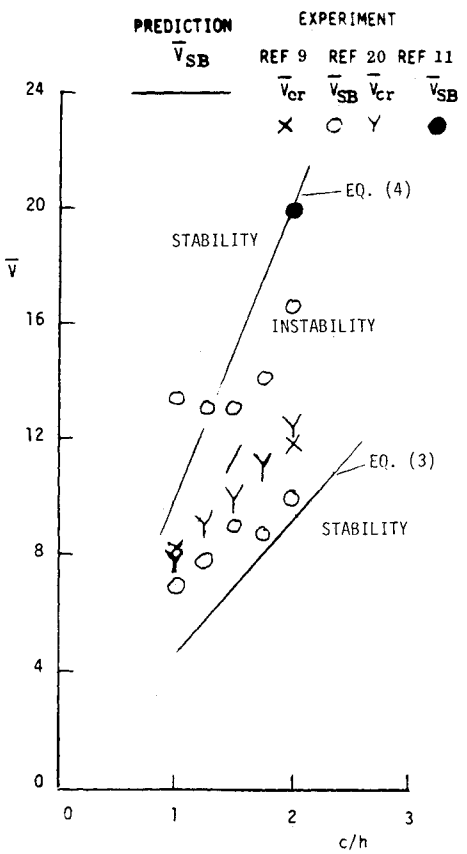

Fig. 12 Conceptual effect of vortex-induced force for torsional oscillations.

back to Fig. 11 one can see that stabilizing vortex-induced effects will exist for $0 < \phi < \pi$, i.e., from $\bar{V}$ given by Eq. (4) to $\bar{V} \to \infty$. This is again in agreement with the experimental results in Fig. 12. Regarding the lower boundary in Fig. 12 (for $\xi_v = 0.25$), Fig. 11 indicates that the next instability would occur for $\phi > 2\pi$, i.e., for $\bar{V} < 2.35$ (c/h). This is in the $\bar{V}$ range for the superharmonic response, which will be discussed later.

It can be seen from Fig. 12 and the analysis leading to Eqs. (3) and (4) that the vortex-induced effects can be as important as the moving-wall effects. The latter are, strictly speaking, not necessary for vortex lock-on on a lift-generating cross section, especially not for torsional oscillations, where the moving-wall effects are decreasing the angle-of-attack effect

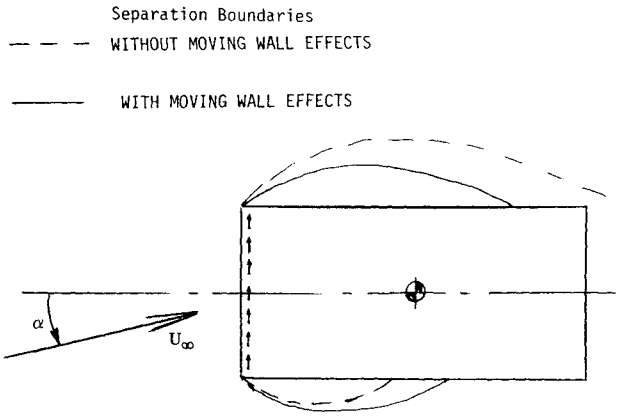

Fig. 13 Moving-wall effect on a pitching rectangular cross section.

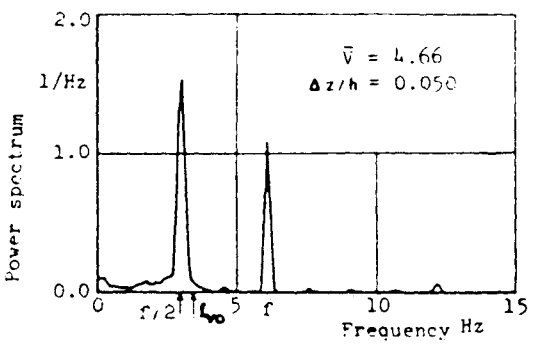

Fig. 14 Power spectrum of square cylinder response.[7]

(Fig. 13), rather than amplifying it, as in the case of plunging or bending oscillations (Fig. 3).

Superharmonic Response

Thus far only the response for oscillations near the Karman vortex shedding frequency has been discussed. It was shown in Ref. 10 that for an oscillating circular cylinder strong response was also possible at three times the Karman vortex shedding frequency. For the cylinder, the moving-wall effect is totally dominant.[17] However, as illustrated, for the rectangular cross section the vortex-induced effect is equally important, and for the torsional oscillations can become the dominant flow mechanism.

The measured power spectrum for the response of a square cross section[7] (Fig. 14) indicates that strong coupling between vortex shedding and body motion is present for $f = 2f_v < 2f_{v0}$. The reason for that must be that the vortex-induced effect dominates for the square cross section, whereas for the circular cylinder the moving-wall effect dominates, giving a strong response at $f = 3f_v$ and only a very weak one at $f = 2f_v$.[10]

For oscillations at twice the Karman vortex shedding frequency the phase lag ϕ will be larger than for the harmonic response discussed earlier. Going back to Fig. 9, one finds that vortex-induced negative aerodynamic damping of bending oscillations will occur first at $\phi < \pi/2$ and then at $3\pi/2 < \phi < 5\pi/2$. The latter condition would be expected to apply for $f = 2f_v$, giving the following instability boundary:

$$1.2(c/h) < \bar{V} < 5.25(c/h) \tag{5}$$

For the low end of the boundary $\xi_v = 0$ was assumed in Eq. (1), and for the high end $\xi_v = 0.7$ was used, the value maximizing the vortex-induced force.[22] Figure 15 shows that the experimentally observed instability region is overpredicted by Eq. (5). To some extent this could be explained by the fact that

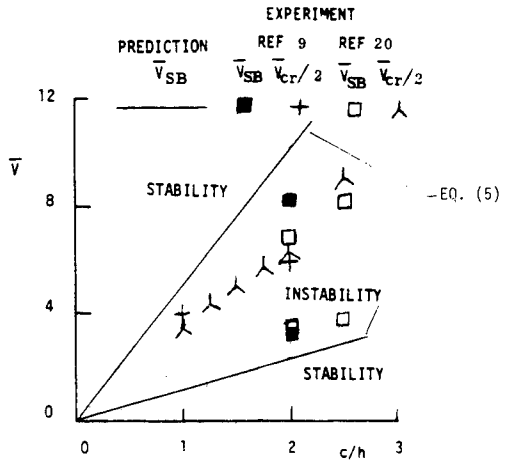

Fig. 15 Stability boundaries at $\alpha=0$ for superharmonic bending response of rectangular cylinders.

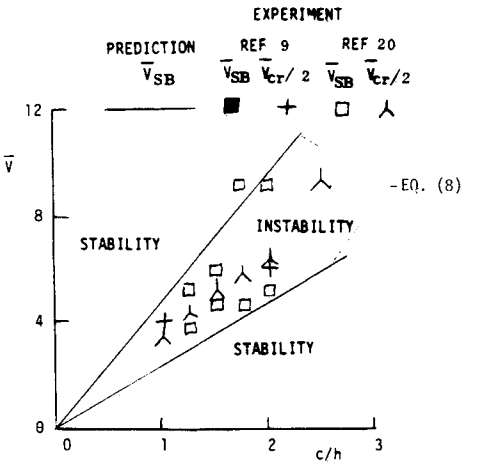

Fig. 16 Stability boundaries at $\alpha=0$ for superharmonic torsional response of rectangular cross sections.

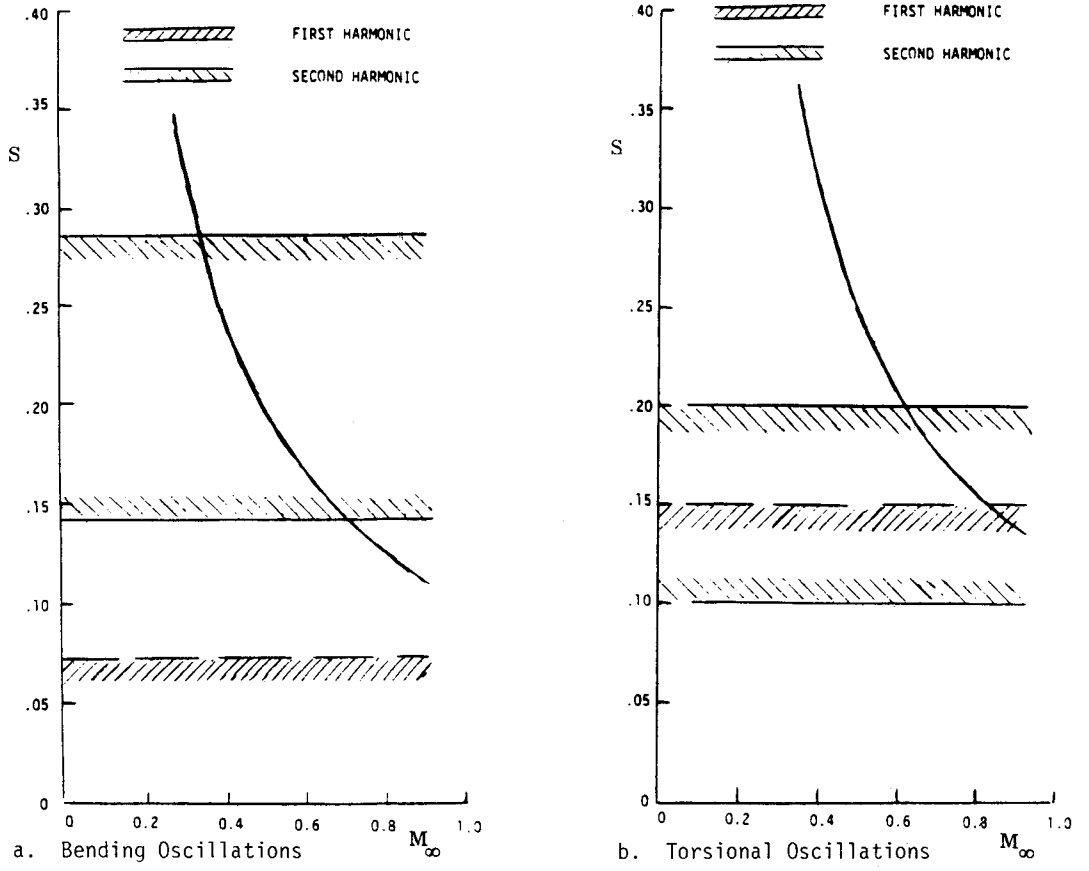

Fig. 17 Stability boundaries for the $c/h\approx 2$ rectangular SRB cable-tray cross section.

the relative influence of the mechanical damping increases strongly with increasing frequency and, therefore, could be large in the superharmonic response.

For the torsional oscillations, Fig. 11 shows that, for the forward vortex location, the second time dynamic instability occurs is for $\phi>2\pi$. The corresponding condition for the aft force location is $\phi<2\pi$. With ξ_v of the harmonic response, Eqs. (3) and (4), respectively, the instability boundaries for the superharmonic response become

$$\bar{V}<2.375(c/h) \tag{6}$$

and

$$\bar{V}>5(c/h) \tag{7}$$

These boundaries are opposite in sign to the experimental ones[19,20] (Fig. 16). What can be the reason for this 180-deg turnaround? Figure 13 gives the clue. If the moving-wall effects dominate over the α effect, the force would be in the opposite direction in Fig. 12. As the moving-wall effects are roughly twice as large as for the harmonic response, it is not unreasonable that they could dominate for the superharmonic response, whereas the regular α effects dominate in the case of the harmonic response. When the moving-wall effects dominate, only the forward force location is applicable, and the first ϕ region for instability, $\pi<\phi<2\pi$, is the one of interest for the superharmonic response. The following instability boundary is obtained when the force is lumped at the

quarter-chord point, as in the case of the harmonic response ($\xi_v = 0.25$):

$$2.375\,(c/h) < \bar{V} < 4.75\,(c/h) \tag{8}$$

Figure 16 shows that the prediction provided by Eq. (8) is in excellent agreement with experiment.[9,20] Initially, this may be a surprise in view of the poorer agreement in the case of bending or plunging oscillations (Fig. 15). One would, of course, expect the lumping of the vortex-induced effect to be a much poorer approximation for the vortex travel effect in the case of torsional oscillations. The answer is that the moving-wall effects dominate for the superharmonic torsional oscillations. To those familiar with the large moving-wall effects observed for the flow separation on axisymmetric bodies at high angles of attack,[26,27] the magnitude of the moving-wall effects required to overcome the α effects (Fig. 13) does not appear to be beyond reach.

Applying the stability boundaries for first and second harmonics of the $c/h = 2$ rectangular cross section gave the lock-in regions shown in Fig. 17 for oscillations of the SRB cable tray in bending and torsional degrees of freedom. It can be seen that favorable interaction from the Karman vortex shedding is obtained for the otherwise divergent torsional oscillations[1,2] at $M_\infty < 0.62$. (Note that negative aerodynamic damping was measured at these moderately high subsonic Mach numbers.[25]) The interaction was, however, unfavorable for the otherwise stable bending oscillations in the speed region $0.62 < M_\infty < 0.72$. Simultaneous lock-in of torsional and bending oscillations is possible in the Mach number range $0.62 < M_\infty < 0.72$.

Based upon the results in Fig. 17, it was decided that the stiff, new SRB cable tray also had to be protected by flow ramps. It should be noted, however, that for flight Mach numbers below 0.62, protective flow ramps probably would not have been needed, since it was the torsional rather than the bending oscillations that produced the critical loading for the cable tray.[1,2] That is, the somewhat surprising result would have been that the interaction from the Karman vortex shedding had eliminated the stall flutter problem which initially prompted the use of protective flow ramps. The bad ring of Karman vortex shedding in the ears of the structural dynamicist stems from the fact that most of the existing experience is for circular cross sections, where the only interaction effect of any consequence is unfavorable. For lifting cross sections, however, the interaction is often favorable in nature.

Conclusions

An analysis of the coupling between Karman vortex shedding and body motion for rectangular cross sections of chord-to-height ratios below 2.5 ($c/h < 2.5$) has shown the following:

1) The moving-wall effect on the flow separation for a rectangular cross section is similar to that for a circular cylinder in regard to bending oscillations.

2) For bending oscillations the vortex-induced effect on the rectangular cross section amplifies the moving-wall effect.

3) For torsional oscillations, however, the vortex-induced effect counteracts the moving-wall effect. At the first harmonic the vortex-induced effect dominates, whereas for the second harmonic the moving-wall effect appears to dominate.

4) The effect of Karman vortex shedding can be beneficial in regard to the structural dynamics. Thus, it eliminates the galloping cable problem for rectangular cross sections over a large velocity range. It also can eliminate the corresponding stall flutter problem for torsional oscillations, as was exemplified in the case of the Space Shuttle solid-rocket booster cable tray.

In regard to three-dimensional flow effects, note the following: for stationary cylinders and for the very small amplitudes not causing vortex lock-on, three-dimensional flow effects are large. However, when the amplitude exceeds a rather modest threshold value, the body motion organizes the flow toward a two-dimensional separation geometry.

Acknowledgments

This paper is based upon results obtained in a study performed under Contract AS2-650323 for the Martin Marietta Corporation, Michoud Operations, with Bud Click as the Contract Coordinator. The author is indebted to his usual coauthor J. P. Reding for helpful discussions, and to Nancy Behney for her help with the manuscript.

References

[1]Ericsson, L. E. and Reding, J. P., "Aeroelastic Stability of Space Shuttle Protuberances," *Journal of Spacecraft and Rockets*, Vol. 19, July-Aug. 1982, pp. 307-313.

[2]Ericsson, L. E. and Reding, J. P., "Aeroelastic Characteristics of the Space Shuttle External Tank Cable Trays," *Journal of Spacecraft and Rockets*, Vol. 22, May-June 1985, pp. 289-296.

[3]Ericsson, L. E. and Reding, J. P., "Stall Flutter Analysis," *Journal of Aircraft*, Vol. 10, Jan. 1973, pp. 5-13.

[4]Ericsson, L. E. and Reding, J. P., "Aeroelastic Stability Analysis of the New SRB Cable Tray," Lockheed Missiles & Space Co., CA, Tech. Rept. LMSC D059412, Contract AS2-650323, May 1983.

[5]Bearman, P. W. and Zdravkovich, M. M., "Flow Around a Circular Cylinder Near a Plane Boundary," *Journal of Fluid Mechanics*, Vol. 89, Pt. 1, 1978, pp. 33-47.

[6]Dyment, A. and Gryson, P., "Etude D'Ecoulements Turbulents Subsoniques et Supercritiques par Visualization Ultra-Rapide," Paper 28, AGARD-CP-227, Sept. 1977.

[7]Bearman, P. W. and Trueman, D. M., "An Investigation of the Flow Around Rectangular Cylinders," *Aeronautical Quarterly*, Vol. 23, Aug. 1972, pp. 229-237.

[8]Parkinson, G. V., "Aeroelastic Galloping in One Degree of Freedom," *Proceedings of the Conference on Wind Effects on Buildings and Structures*, National Physics Laboratory, England, June 1963, Vol. II, Her Majesty's Stationery Office, London, 1965, pp. 582-609.

[9]Nakamura, Y. and Mizota, T., "Unsteady Lifts and Wakes of Oscillating Rectangular Prisms," *Journal of the Engineering Mechanics Division, ASCE*, Vol. 101, No. EM6, Dec. 1975, pp. 855-871.

[10]Ericsson, L. E., "Karman Vortex Shedding and the Effect of Body Motion," *AIAA Journal*, Vol. 18, Aug. 1980, pp. 935-944.

[11]Nakamura, Y. and Mizota, T., "Torsional Flutter of Rectangular Prisms," *Journal of the Engineering Mechanics Division, ASCE*, Vol. 101, No. EM2, April 1975, pp. 125-143.

[12]Ericsson, L. E., "Limit Amplitude of Galloping Cables," *AIAA Journal*, Vol. 22, April 1984, pp. 493-497.

[13]Ericsson, L. E., "Hydroelastic Effects of Separated Flows," *AIAA Journal*, Vol. 21, March 1983, pp. 452-458.

[14]Novak, M. "Galloping and Vortex Induced, Oscillations of Structures," *Proceedings of the Third International Conference on Wind Effects on Buildings and Structures*, Saicon Co., Ltd., Tokyo, Japan, Sept. 1971, pp. 799-809.

[15]Ferguson, M. and Parkinson, G. V., "Surface and Wake Phenomena of the Vortex-Excited Oscillation of a Circular Cylinder," *Journal of Engineering for Industry*, Vol. 89, No. 3, Nov. 1967, pp. 831-838.

[16]Ericsson, L. E., "Maximum Crossflow Response of a Circular Cylinder, a Non-Resonant Flow Phenomenon," AIAA Paper 84-0422, Jan. 1984.

[17]Ericsson, L. E., "Circular Cylinder Response to Karman Vortex Shedding," AIAA Paper 86-0999-CP, May 1986.

[18]Ericsson, L. E., "Effect of Cross-sectional Shape on the Response to Karman Vortex Shedding," AIAA Paper 85-0448, Jan. 1985.

[19]Parkinson, G. V., "Aeroelastic Galloping, in One Degree of Freedom," *Proceedings of the Conference on Wind Effects on Buildings and Structures*, National Physics Laboratory, England,

June 1963, Vol. II, Her Majesty's Stationery Office, London, 1965, pp. 582-609.

[20]Otsuki, Y., Washizu, K., Tomizawa, H., Ohya, A., and Fujii, K., "Experiments on the Aeroelastic Stability of Prismatic Bars with Rectangular Sections," *Proceedings of the Third International Conference on Wind Effects on Buildings and Structures*, Saikon Co., Ltd., Tokyo, Japan, Sept. 1971. pp. 891-898.

[21]Ericsson, L. E. and Reding, J. P., "Dynamic Stall Analysis in Light of Recent Numerical and Experimental Results," *Journal of Aircraft*, Vol. 13, April 1976, pp. 248-255.

[22]Ericsson, L. E. and Reding, J. P., "Dynamic Stall at High Frequency and Large Amplitude," *Journal of Aircraft*, Vol. 17, March 1980, pp. 136-142.

[23]Carta, F. O., "Analysis of Oscillatory Pressure Data Including Dynamic Stall Effects," NASA CR-2394, May 1974.

[24]Carta, F. O., "Chordwise Propagation of Dynamics Stall Cells for an Oscillating Airfoil," AIAA Paper 75-25, Jan. 1975.

[25]Orlik-Rückemann, K. J. and LaBerge, J. G., "Dynamic Wind Tunnel Tests of the Simulated Shuttle External Tank Cable Trays," *Journal of Spacecraft and Rockets*, Vol. 20, Jan.-Feb. 1983, pp. 5-10.

[26]Ericsson, L. E. and Reding, J. P., "Steady and Unsteady Vortex-Induced Asymmetric Loads on Slender Vehicles," *Journal of Spacecraft and Rockets*, Vol. 18, March-April 1981, pp. 97-109.

[27]Ericsson, L. E. and Reding, J. P., "Dynamics of Forebody Flow Separation and Associated Vortices," *Journal of Aircraft*, Vol. 22, April 1985, pp. 329-335.